



Stress distributions around the interference fit between a round pin and a perforated finite plate

D. Castagnetti¹ · E. Dragoni¹

Received: 13 November 2023 / Accepted: 19 February 2024
© The Author(s) 2024

Abstract

Interference fit couplings between a perforated finite plate and a round pin are widely used mechanical systems in several industrial applications. Only a few works in the literature investigate the coupling contact pressure due to interference in the absence of an external load, and these works are limited to a few specific configurations. To overcome this limitation, this work performs a numerical systematic investigation of the pin-plate coupling for a wide range of configurations that can be encountered in practice. Three are the variables investigated: the pin diameter, the plate length, and the pin offset in the longitudinal direction, all of them normalized over plate width, for a total of 18 configurations. The work provides a detailed prediction of the contact pressure and equivalent von Mises stress along the contact surface and compares the results with photoelastic investigations retrieved from the literature. For design purposes, the results are synthesized through two stress concentration factors, one referring to the peak contact pressure, and the second one to the peak von Mises stress.

Keywords Interference fit · Pin · Finite plate · Contact pressure · Stress concentration

1 Introduction

The work investigates the contact stresses due to interference between a cylindrical pin and a rectangular plate with finite dimensions, with particular focus on the contact pressure distribution.

This configuration is largely used in many mechanical applications, such as fork-pin-rod joints and riveting. A peculiar application concerns the creation of torsion specimens for the shear strength characterization of hybrid joints, press-fitted and bonded with adhesive.

In the literature there are some works that investigate, for a few specific configurations, the contact pressure due to the interference between a pin and a finite rectangular plate, in the absence of applied external loads. Heywood

[1] investigates the effect of an unloaded pin, fitted into a hole in a tensile plate: he observes that the restraining effect exerted by the pin on the hole deformation (transverse diameter reduction) has a beneficial effect on the stress concentration factor produced by the hole in the plate. Lambert [2] compares the experimental stress distribution (photoelastic model) in a rectangular plate due to an interference fit pin, with the analytical prediction from the Lamé theory, showing a close agreement up to a 0.6 ratio between pin diameter and plate width. Solodovnikov [3] proposes a solution for the contact problem of a rectangular elastic plate with a circular hole loaded in tension, with a pin of circular cross section fitted into it: the model takes into account friction and a tensile load on the plate.

Other works, always for specific configurations, analyse the contact pressure between pin and a finite plate when subjected to an external load acting in the longitudinal plane of the plate [Jessop et al. [4], Cox et al. [5], Rao et al. [6], Mather et al. [7], Rao [8], Murthy et al. [9]]. Goel et al. [10] perform a numerical thermo-mechanical analysis to evaluate the effect of the insertion process in an interference fit pin-plate connection. Two works from Ciavarella et al. [11, 12] propose a closed-form solution to the contact problem between a loaded pin and an infinite plate, for the general case of elastically similar materials in frictionless

Technical Editor: João Marciano Laredo dos Reis.

✉ D. Castagnetti
davide.castagnetti@unimore.it
E. Dragoni
eugenio.dragoni@unimore.it

¹ Department of Science and Methods for Engineering,
University of Modena and Reggio Emilia, Via G. Amendola
2, Reggio Emilia, Italy

contact. A similar approach is proposed by Hou et al. [13, 14], while Iyer [15] compares the solutions from Ciavarella [11, 12] and Hou et al. [13, 14] with the predictions from a finite element model describing the same configuration (infinite plate) but realistic contact conditions (friction coefficient). Specifically, he observed that the increase of friction coefficient reduces the peak contact pressure and increases the stress concentration in the plate. Croccolo et al. [16] extended the analytical calculation of pin hub couplings to configurations including more than 2 elements. Pedersen [17] and Strozzi et al. [18] investigate the case of a shrink fit between a solid shaft and a hub focusing on the effect of geometry to optimize contact stresses. Malavolta et al. [19] provide an analytical formulation to predict the influence of thermo-mechanical stress state on the torque capacity of rotating interference fit assembly. Foust et al. [20] investigate the stresses in a pinned wood joint configuration through grey field photoelasticity. Wu et al. [21] propose an analytical method to calculate stress around interference fit holes on composite pinned plates under tensile load. Imran et al. [22] investigate the contact stress distribution of centrally holed plate for different interference fit levels. Karmankar [23] numerically predicts the stresses in a pin-plate coupling for different interference levels. Pedersen [24] numerically investigates the stress concentration factor and the optimal design of pinned connections. Booker et al. [25] study the various factors which influence the capacity of interference-fitted couplings including modelling approaches, coefficient of friction, surfaces, the geometry, materials, loading and the assembly process. Two recent works from Radi et al. [26] and from Strozzi et al. [27] analyse pin-lug connections and propose an analytical 2D solution to predict the stress and displacement fields under the assumption of frictionless contact and clearance.

It emerges that a systematic analysis of the contact stresses due to the interference fit between a pin and a finite rectangular plate without any external load applied, for a wide range of dimensional ratios, cannot be retrieved.

The present work aims to overcome this drawback by carrying out a set of numerical analyses to investigate the whole range of possible configurations that can be encountered in practice. The numerical analyses focused on 2D finite element models, since the aim of this work was to investigate the distribution of the contact stresses in the circumferential direction, disregarding the highly localized stress concentrations, which occur on the boundaries in the axial direction. As can be observed in several works from the literature [22, 28–32], the investigation of these stress peaks requires a very detailed, computationally expensive numerical model, and are strongly affected by the details of the geometry (fillets or chamfers on the hub). This test plan will examine the following variables, while keeping constant the width of the rectangular plate: the ratio between pin diameter and plate

width, aspect ratio of the plate, pin offset along the longitudinal axis of the plate.

The analyses are carried out by implementing a plane stress finite element model, which exploits the symmetry of the system and describes a frictionless contact. The results show an excellent agreement with the experimental photoelasticity maps from the literature and show how the contact stresses become less uniform in the circumferential direction by increasing the diameter of the pin with respect to the size of the plate and as the pin offset becomes higher.

The outcome is significant for the development of a compact specimen where the contact interface is subjected to shear stresses promoted by a torsional load applied to the plate and acting about the pin axis.

2 Method

2.1 Numerical test plan

Figure 1 shows the sketch of the pin-plate configuration investigated in the work, where d represents the pin diameter, e the offset between pin centre and plate midpoint along the length L of the plate, B the width of the plate. To perform a systematic investigation, we set the width of the plate B equal to 40 mm and considered the three dimensionless ratios in Table 1: the ratio of the pin diameter d to the width of the plate B (over three levels); the ratio of the length

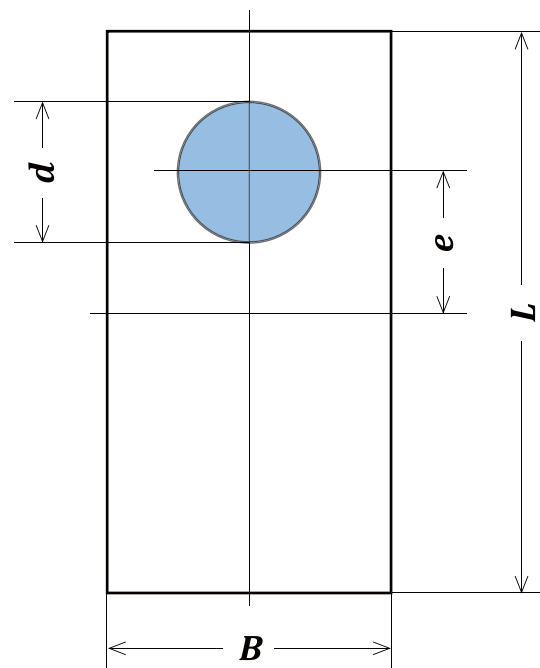


Fig. 1 Sketch of the pin-plate configuration investigated in the work with main dimensions

Table 1 Variables of the numerical investigation

d/B	0.25	0.5	0.75		
L/B	1	1.5	2	2.5	3
e/B	0	0.25	0.5		

of the plate L to the width of the plate B (over five levels); the ratio of the offset e to the width of the plate B (over three levels). By excluding the offset ratios giving inconsistent or redundant configurations, we obtained the 18 geometries displayed in Fig. 2.

We highlight that the high d/B ratio (equal to 0.75) has been considered to provide a comprehensive investigation, which includes all the ratios which could eventually occur in real applications. Compared to a small hole in a large

plate, a large d/B ratio reduces the stress concentration factor originated by the hole in the plate, giving a more uniform stress distribution. This configuration is preferred also in case we need a plate which bears a lower load than the pin. In addition, the high d/B ratio for the pin-plate coupling is of interest for the development of a compact torsion specimen, where the plate acts like a lever on the pin, and the contact interface is subjected to shear stresses only.

2.2 Finite element model

As described in Fig. 3a, the finite element model exploited the symmetry of the structure, with respect to the vertical axis for all the configurations, and with respect to the horizontal axis for configurations with no offset of the pin. Thus, the model describes half or a quarter of the structure. The

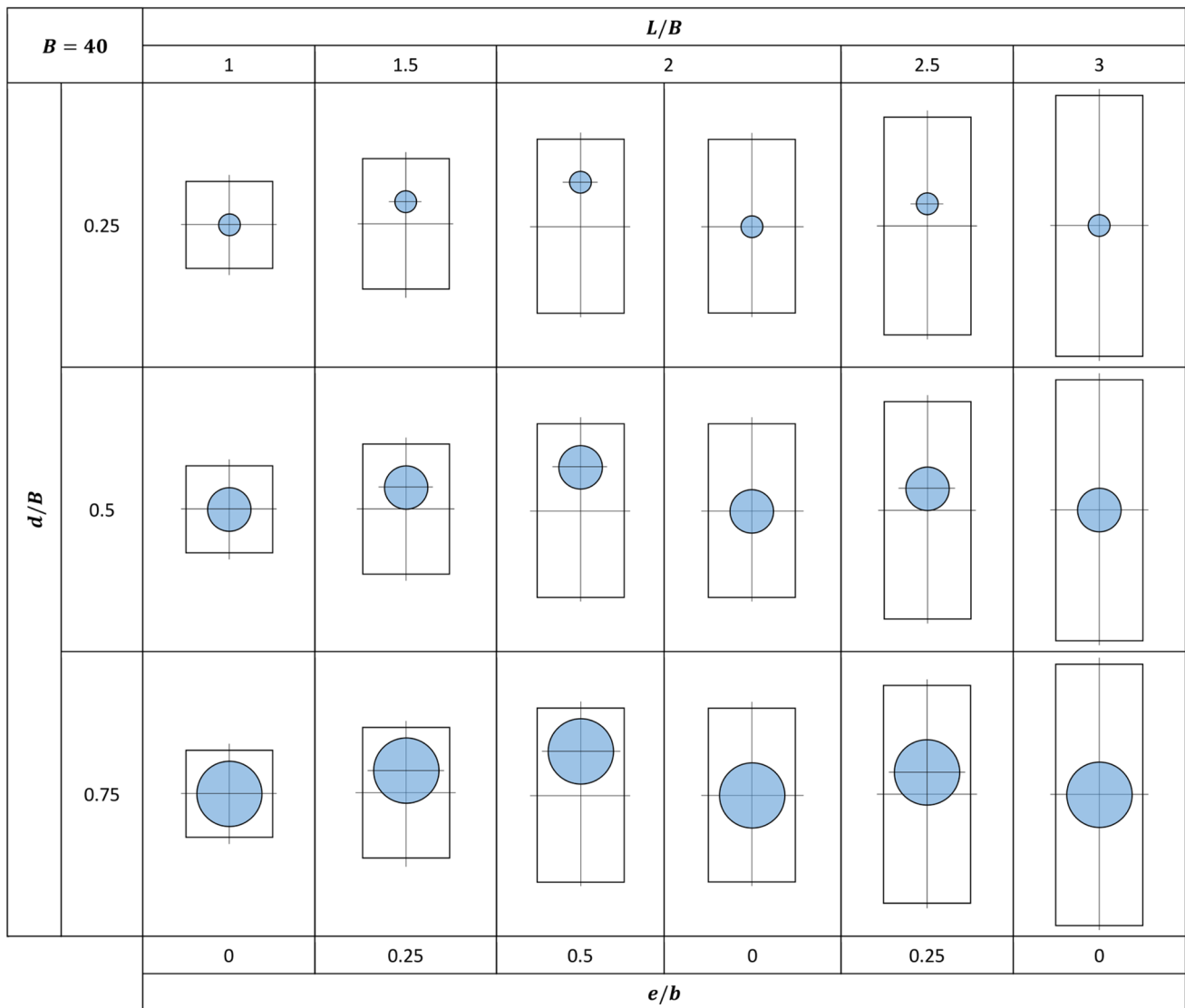
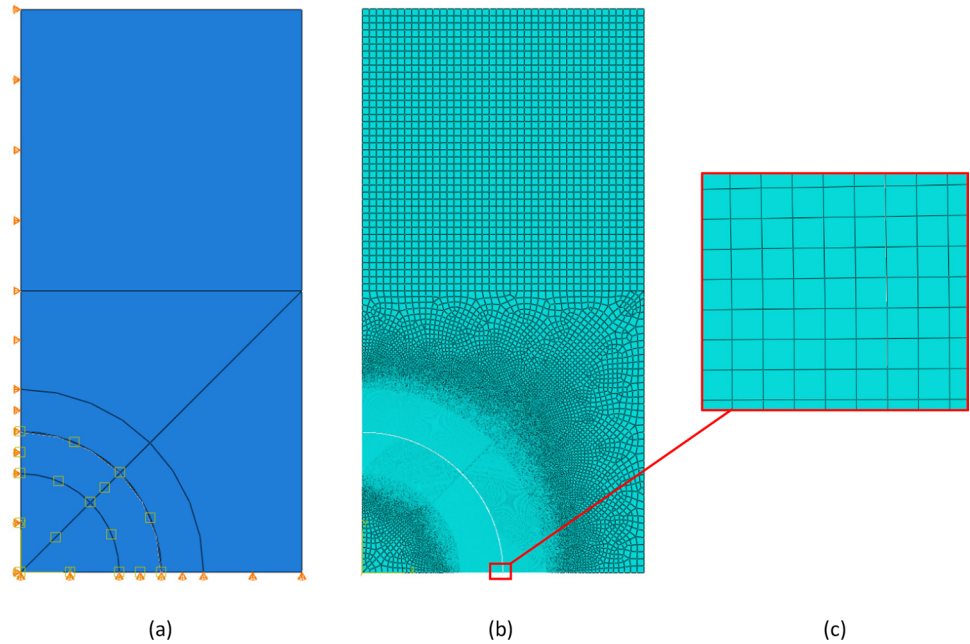


Fig. 2 Sketch of the 18 configurations investigated numerically

Fig. 3 Finite element model: geometry, temperature field in the pin, and symmetry constraints (a); overall view of the mesh (b); close-up view of the mesh in the contact region (c)



model assumes a plane stress behaviour for the pin-plate coupling, using 4-noded, bilinear, plane stress quadrilateral elements (CPS4 [33]). A minimum side length equal to 0.02 mm was used for the elements on the contact interface (Fig. 3b, c), as a result of the convergence analysis presented below. Specifically, to improve the accuracy the model applies nearly-square quadrilateral elements across the contact interface. The model describes both the pin and the plate as linearly elastic materials with the typical properties of steel (Young's modulus = $E = 206$ GPa, Poisson's ratio = $\nu = 0.3$, coefficient of thermal expansion $\alpha = 1.2\text{E-}5$ K^{-1}): we highlight that these parameters were chosen as the most usual for this class of interference-fit coupling, but any other set of values could be used without changing the trend of the results. A frictionless contact was implemented at the interface, with a "hard" contact pressure-overclosure law [33]. The assumption of a frictionless contact, which allows to simplify the finite element model, is supported by the fact that the relative displacement between the pin and plate contact surfaces is nearly zero. This comes from the fact that the unique load on the system is given by the interference fit, while no external load is applied to the pin, and also the plate is unloaded. Thus, the friction coefficient does not play any effect on the stress field of the components. This assumption was also validated by comparison with a finite element model (not shown here for the sake of clarity), which sets the friction coefficient to 0.25 (a representative value for a metal-to-metal contact): all the results retrieved from the analysis were coincident to those from the same model with a frictionless contact. The interference between pin and plate, was produced virtually by means of a uniform temperature increase applied to the pin.

To allow for a straightforward comparison and normalization of the results, for all the configurations investigated, the temperature applied to the pin was chosen to generate a contact pressure equal to 100 MPa in a simplified pin-hub coupling as represented in Fig. 4a (pin inserted in a cylinder with outside diameter $D = B$, where B is the width of the plate). The relationship between temperature change and contact pressure can be derived as follows.

The temperature rise of the pin, T , needed to generate a virtual diametral interference, δ , with the hole must satisfy the following condition [34]:

$$\alpha dT = \delta \quad (1)$$

The contact pressure, p , generated by an interference δ between a solid pin of diameter d and a hub of outside diameter B is (Budynas et al.[35]):

$$p = E \frac{\delta}{d} \frac{1 - \left(\frac{d}{D}\right)^2}{2} \quad (2)$$

Letting $D = B$ in (2), combining with (1) and simplifying gives

$$T = \frac{2p}{E\alpha} \cdot \frac{B^2}{B^2 - d^2} \quad (3)$$

Equation (3) supplies the temperature rise of the pin capable of generating the prescribed nominal contact pressure p (= 100 MPa) between pin and plate.

According to the classical thick pressure vessel theory, the principal stresses in the hub, on the hole surface, are the hoop and radial stresses, given by (Budynas et al.[35]):

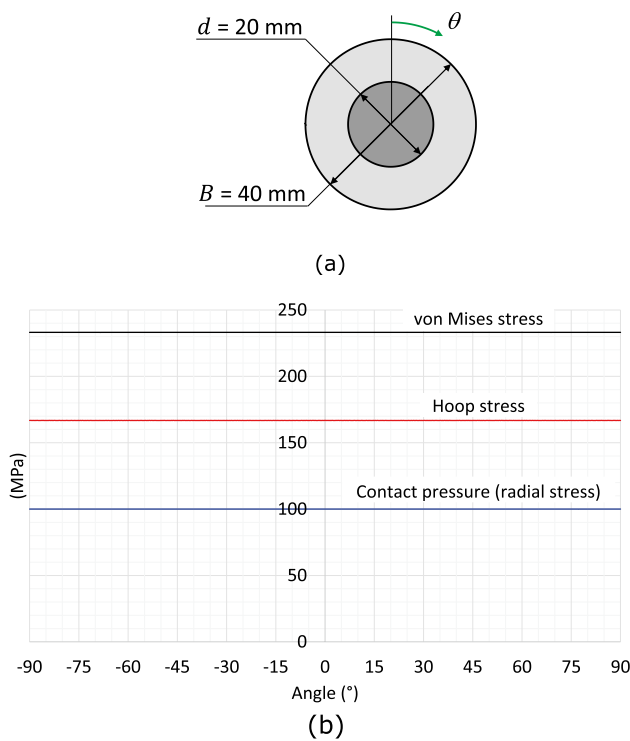


Fig. 4 Pin-hub coupling used for calibration of the finite element model: sketch of the model (a), and numerical prediction of the contact pressure, hoop stress and equivalent von Mises stress

$$\sigma_1 = \sigma_c = p \frac{1 + \left(\frac{d}{B}\right)^2}{1 - \left(\frac{d}{B}\right)^2} \tag{4}$$

$$\sigma_2 = \sigma_r = -p \tag{5}$$

It comes that the equivalent von Mises stress in that region can be written as:

$$\sigma_{\text{vonMises}} = \sqrt{\sigma_c^2 + \sigma_r^2 - \sigma_c \sigma_r} \tag{6}$$

Introducing (4) and (5) into (6) and simplifying gives:

$$\sigma_{\text{vonMises}} = \frac{p}{1 - \left(\frac{d}{B}\right)^2} \sqrt{3 + \left(\frac{d}{B}\right)^4} \tag{7}$$

The configuration in Fig. 4a was used to perform the convergence analysis of the finite element model, giving an element side length of 0.02 mm on the contact interface, as described above.

For this pin-hub coupling configuration, the blue curve in Fig. 4b shows the accurate prediction of the contact pressure as a function of the angular position (i.e., the radial stress). Similarly, the red and the black curves

describe the hoop stress and the equivalent von Mises stress predicted by the finite element model. These three values, which are obviously constant along the whole contact surface, coincide with the values predicted by Eqs. (4), (5), and (7), respectively.

3 Results

Figure 5 displays the results for two pin-plate couplings in terms of contact pressure (left column) and equivalent von Mises stress (right column): Fig. 5a, b refer to the configuration with $d = 10\text{mm}$, $L = 40\text{mm}$, and $e = 0\text{mm}$, while Fig. 5c, d refer to the configuration with $d = 30\text{mm}$, $L = 60\text{mm}$, and $e = 10\text{mm}$.

Figure 6 presents three graphs displaying the finite element prediction of the contact pressure profiles along the interface, as a function of the angular coordinate. Each plot collects the six curves corresponding to one of the pin diameters investigated in the test plan: $d = 10\text{mm}$ in Fig. 6a, $d = 20\text{mm}$ in Fig. 6b, $d = 30\text{mm}$ in Fig. 6c, while different type of lines and thicknesses values are used to distinguish the length of the plate L , and the offset e . For each plot, we reported a black line, which represents the numerical contact pressure for the reference pin-hub configuration with the same d/B ratio of that set.

With the same layout as in Figs. 6, 7 displays the finite element prediction of the equivalent von Mises stress along the contact interface of the plate ($d = 10\text{mm}$ in Fig. 7a, $d = 20\text{mm}$ in Fig. 7b, $d = 30\text{mm}$ in Fig. 7c). For each plot we reported a black line, which represents the analytical von Mises stress for a pin-hub configuration with the same d/B ratio of that set. The analytical von Mises stress was calculated according to Eq. (7).

For three configurations, Fig. 8 compares the photoelastic measurements performed by Lambert[2] (left side) on a plate with a length $L = 10$ inches, and zero offset e of the pin, with the finite element predictions of Tresca equivalent stress (right side) obtained in the present work: Fig. 8a focuses on a configuration with a diameter over plate width ratio $d/B = 0.25$, while in Fig. 8b and c the configurations are quite close but not identical in terms of d/B ratio.

Figure 9 presents the stress concentration factor in the coupling as a function of the pin diameter over plate width ratio. Specifically, we calculated the stress concentration factor in two ways: firstly, the solid circles display the ratio between the peak contact pressure value for the 18 configurations in Fig. 6 and the reference configuration (pin-hub coupling, $p = 100$ MPa, Fig. 4), namely $k_{t,p}$. Secondly, the crosses display the ratio between the peak von Mises stress values in the curves in Fig. 7 and the constant von Mises stress value in the corresponding reference configuration

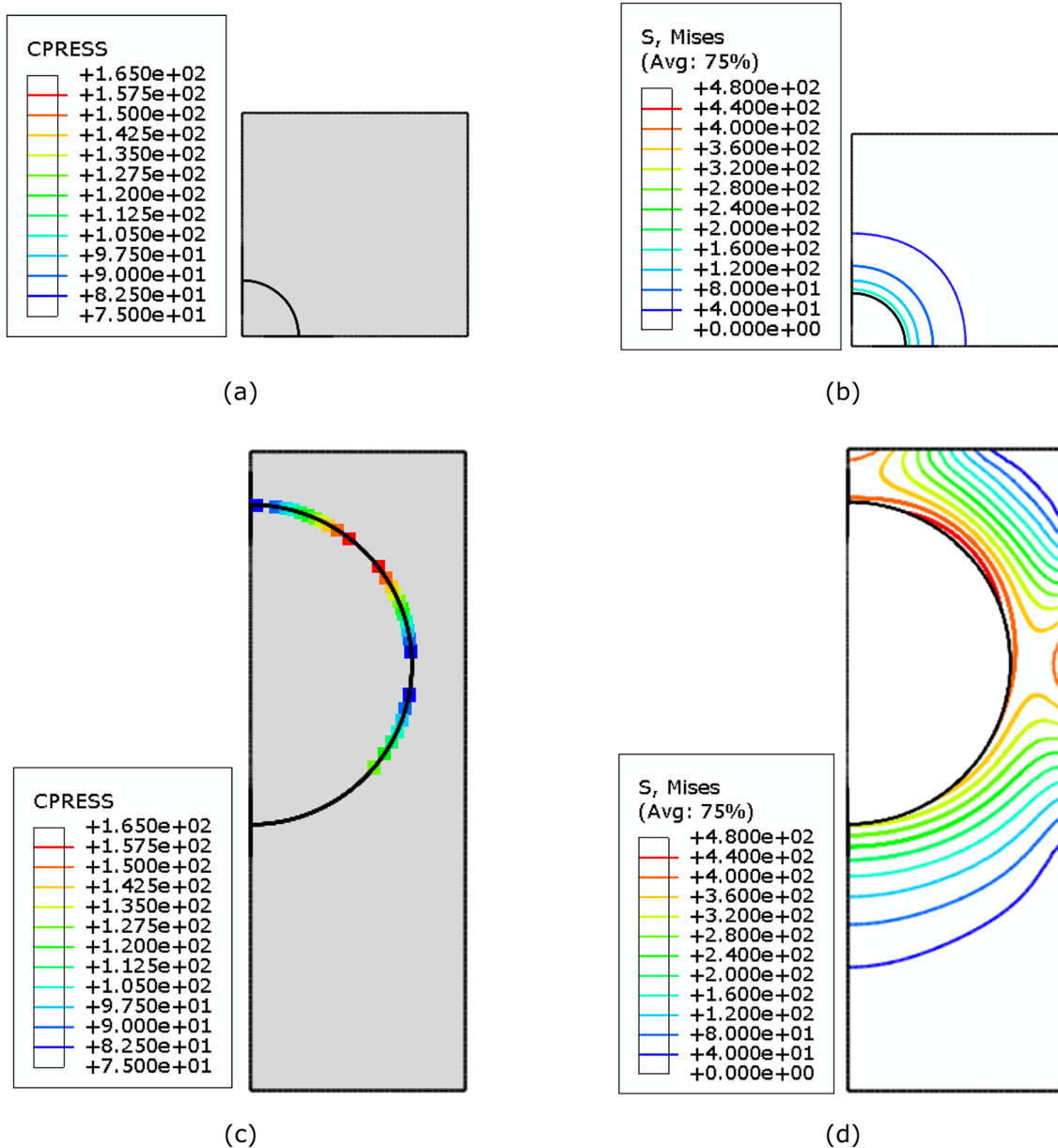


Fig. 5 Contact pressure (left column, N/mm^2) and equivalent von Mises stress (right column, N/mm^2) for two pin-plate coupling configurations: $d = 10\text{mm}$, $L = 40\text{mm}$, and $e = 0\text{mm}$ (a), (b); $d = 30\text{mm}$, $L = 60\text{mm}$, and $e = 10\text{mm}$ (c), (d)

(same d/B ratio, solid black lines in Fig. 7), namely $k_{t,\text{vonMises}}$

4 Discussion

The contour maps in Fig. 5 provide a clear trend of the contact pressure and equivalent von Mises stress for two remarkably different coupling configurations. The configuration in the first row (Fig. 5a, b), featuring a small pin diameter in the centre of a square plate, exhibits a nearly uniform contact pressure (Fig. 5a), with a value quite close to 100 MPa: this

value equals that of the reference pin-hub configuration in Fig. 4. It comes that also the equivalent von Mises stress in Fig. 5b is quite uniform in the circumferential direction, while decreasing in the radial one. However, it is worth noting to observe that the maximum value (about 190 MPa) is nearly equal to that of the pin-hub configuration with the same d/B ratio (about 185 MPa, see the corresponding black curve in Fig. 7).

Quite less uniform is the contact pressure trend for the configuration in Fig. 5c, where the large ratio of the pin diameter over the plate width makes the plate stiffness significantly different along the circumferential direction.

Fig. 6 Contact pressure as a function of the angle for all the configurations investigated in the test plan: $d = 10\text{mm}$ (a), $d = 20\text{mm}$ (b), $d = 30\text{mm}$ (c), solid black line represents the reference pin-hub coupling

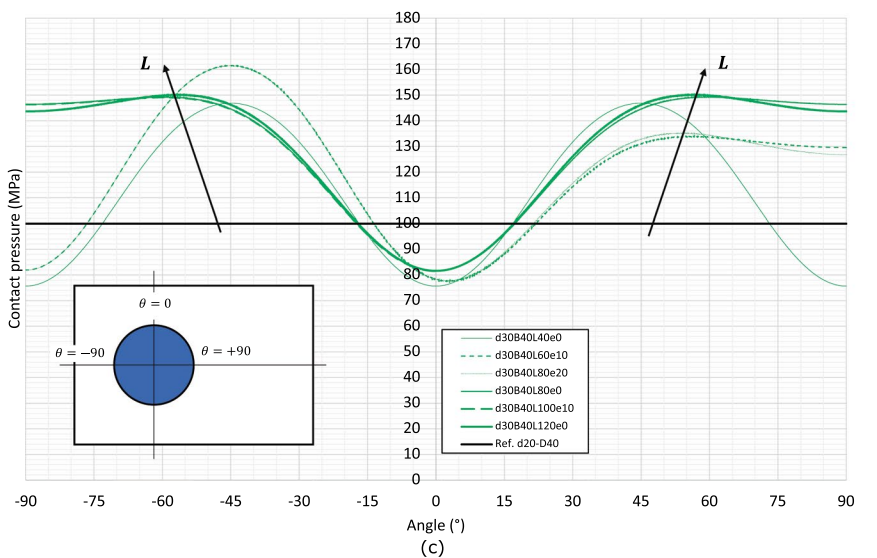
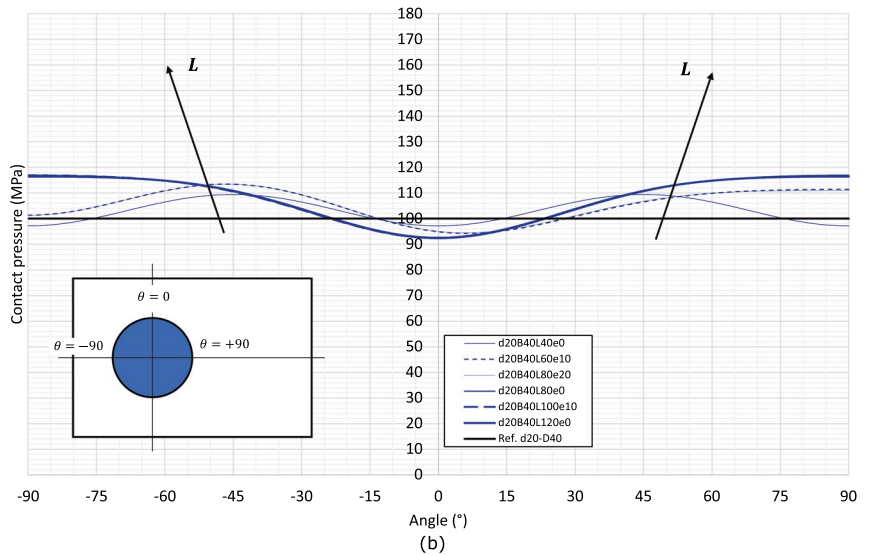
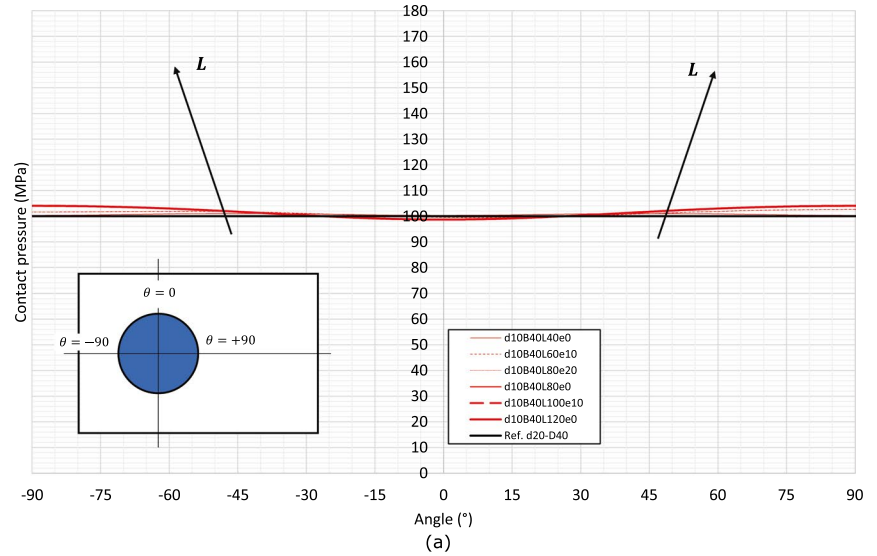
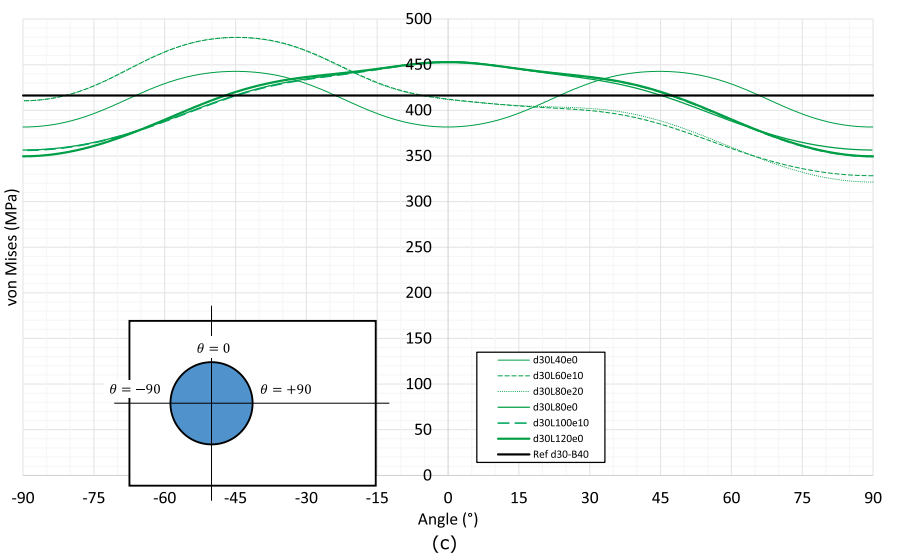
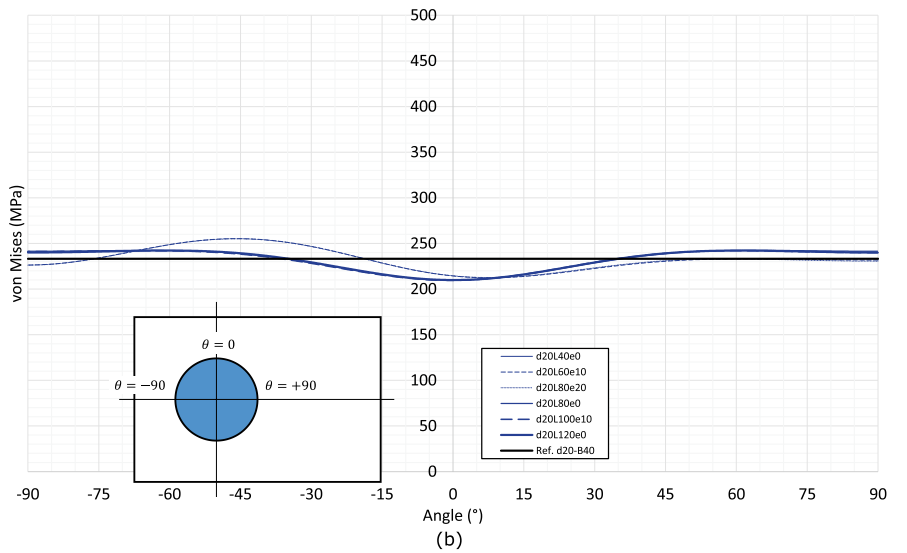
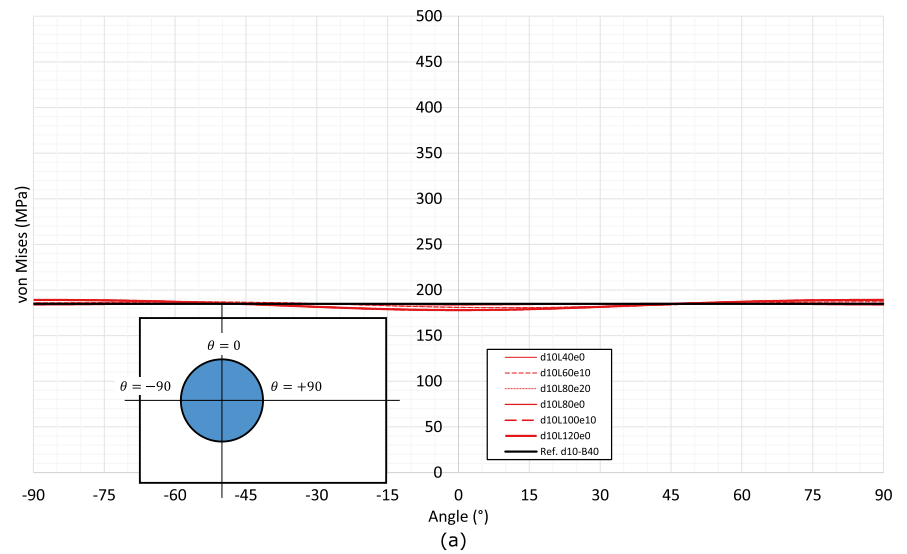


Fig. 7 Equivalent von Mises stress along the contact interface of the plate, as a function of the angle for all the configurations investigated in the test plan: $d = 10\text{mm}$ (a), $d = 20\text{mm}$ (b), $d = 30\text{mm}$ (c), solid black lines represent the analytical von Mises stress for the three reference configurations of the pin-hub coupling ($d/B = 0.25, 0.5, 0.75$)



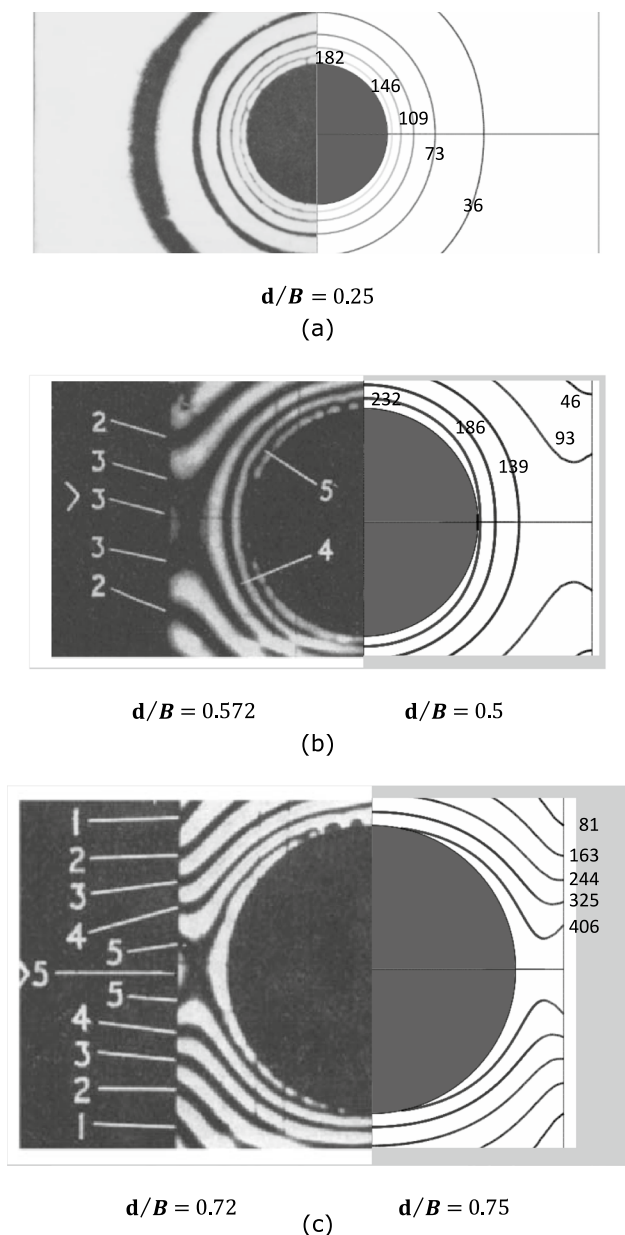


Fig. 8 Comparison between the photoelastic measurements performed by Lambert [2] (left side) for three different configurations and the finite element predictions of Tresca equivalent stress (right side) obtained in the present work, for the same **a** or quite similar **b** and **c** configurations. Numerical values on the right correspond to the Tresca stress values of contour lines in MPa

Specifically, we observe a minimum contact pressure value in the bottom part of the contact interface, since the plate is locally stiffer than elsewhere, and displaces the pin upward. In the horizontal as in the vertical direction, due to the low thickness (i.e., local low stiffness) of the plate the contact pressure is again low, while it reaches a maximum at an angle of 45° from the horizontal direction, due to the high radial thickness (i.e., high local stiffness) of the plate.

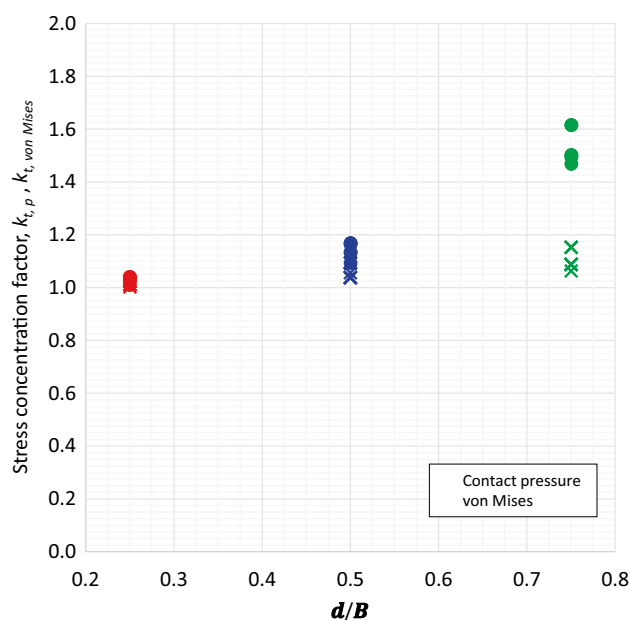


Fig. 9 Stress concentration factor plotted as a function of the pin diameter over plate width ratio calculated from peak contact pressure values, $k_{t,p}$ (solid circles), and from peak von Mises stress values, $k_{t,vonMises}$ (crosses)

The contour plot of equivalent von Mises stress in Fig. 5d describes a similar behaviour: the bottom region of the plate exhibits low stress values, while the regions with minimum plate thickness (along the horizontal and vertical directions) show a nearly uniform high stress throughout. On the bisector of the first quadrant, where the contact pressure reaches its maximum, a peak equivalent von Mises stress arises at the hole surface.

The curves of the contact pressure in Fig. 6 confirm the trend observed for the two configurations in Fig. 5. The red curves in Fig. 6a, which refer to the pin diameter $d = 10$ mm (i.e. $d/B = 0.25$), describe a contact pressure quite close to the reference value of 100 MPa on the whole contact interface, with a negligible effect of the length of the plate L and the offset e of the pin.

The blue curves in Fig. 6b, pin diameter $d = 20$ mm (i.e., $d/B = 0.5$), exhibit a contact pressure oscillation along the contact circumference which ranges from about 92.5 MPa up to 115 MPa for the configuration with $L = 120$ mm and $e = 0$ (continuous thick blue line). In addition, the effect of the plate length L and the pin offset e is non negligible. On the one hand, compared to the square plate, a higher length causes the contact pressure to significantly increase on the left ($\theta = -90^\circ$) and right side ($\theta = 90^\circ$) end of the contact interface (continuous thin vs thick blue curves): this can be imputed to the higher stiffness of the plate sides. On the other hand, the pin offset makes the contact pressure distribution non symmetric between the

left side ($\theta = -90^\circ$) and the right side ($\theta = 90^\circ$) of the plate (dashed vs continuous lines): this comes from the significant difference in the plate stiffness between the left and right side of the coupling.

The green curves in Fig. 6c, pin diameter $d = 30$ mm (i.e., $d/B = 0.75$) highlight a strong amplification of the effects described above: the contact pressure along the interface ranges from a minimum of about 75 MPa up to a peak more than 160 MPa for the configuration with $L = 80$ MPa and $e = 20$ (dotted thin green line). This testifies a remarkable oscillation compared to the reference value of the pin-hub coupling in Fig. 4. The increase of the plate length L and the pin offset e confirms their effect as highlighted for the blue curves ($d = 20$ mm) in terms of the contact pressure increase in the tails of the distribution and also with regard to the asymmetry of the distribution between left and right side.

The trend of the equivalent von Mises stress curves in Fig. 7 resembles that of the contact pressure in Fig. 6. For the lower d/B ratio (red curves in Fig. 7a), the numerical von Mises stress on the hole surface of the plate is nearly constant and very close to the analytical value of the corresponding pin-hub coupling. The blue curves in Fig. 7b ($d/B = 0.5$) exhibit a small oscillation across the analytical reference value and a low asymmetry between left ($\theta = -90^\circ$) and right side ($\theta = 90^\circ$) in case the pin offset is different from zero (dashed curves). For the higher d/B ratio (green curves in Fig. 7c), both the oscillation across the reference value (pin-hub coupling $d/B = 0.75$) and asymmetry between left and right hand in case of non-zero pin offset (dashed curves) are quite strong. On the one hand, the symmetric configurations exhibit a peak von Mises stress for $\theta = 0^\circ$, where the radial thickness of the plate is minimum. On the other hand, the asymmetric configurations show a peak von Mises stress at $\theta = -45^\circ$, due to the peak contact pressure in that same place (see Fig. 6).

The comparison between photoelastic measurements and finite element predictions in Fig. 8, which focuses on three pin-plate coupling configurations, provides a clear assessment of the accuracy of the finite element model in predicting the response of the system.

Despite a small difference between experimental and numerical configurations in Fig. 8b and c (a smaller d/B ratio in Fig. 8c, and a larger one in Fig. 8c on the numerical side), we can observe an excellent agreement between the experimental and numerical fringe patterns: the same number, position, and shape for all the three cases.

Thanks to the calculation of the stress concentration factors kt , p and kt , von Mises, Fig. 9 provides an overall synthesis of the numerical results for design purposes. It is worth noting that in terms of peak contact pressure (solid circles in Fig. 9), we have a significant increase over the value of the reference configuration only for a d/B ratio equal to 0.5 or larger. Specifically, the peak contact

pressure is about 15% higher than the reference one for $d/B = 0.5$, while it reaches more than 50% for $d/B = 0.75$.

From the stress concentration factor calculated upon the von Mises stress (crosses in Fig. 9), appears an interesting result: the stress concentration is quite low for all the three pin diameter over plate width ratios, ranging from a value slightly higher than one for $d/B = 0.25$, up to a value of about 1.15 for $d/B = 0.75$. The trend as a function of the d/B ratio is linear, and some differences emerges between the different configurations as this ratio increases. This parameter proves that the stress field of the pin-plate coupling is nearly the same as for the pin-hub coupling, although a small concentration can be observed in the pin-plate coupling, specifically at a high d/B ratio.

The plot of the average contact pressure in Fig. 10 shows that the average contact pressure is much lower than the peak contact pressure, while at the same time it is higher than the nominal contact pressure of 100 MPa of the reference pin-hub coupling: this testifies a higher pull-out capacity of the joint. At the same time, the trend of the contact pressure for the three levels of the d/B ratio is quite similar to that of the equivalent von Mises stress (crosses in Fig. 9); thus, this higher contact pressure is directly linked to the higher stress state in the material.

On the whole, these results provide a thorough insight into the mechanical response of the pin-plate coupling, for different dimensional ratios, and pin offset values. Specifically, the exact knowledge of the contact pressure variation along the circumferential direction, as well as the von Mises stress in the plate, are the basis for a rational design of the coupling.

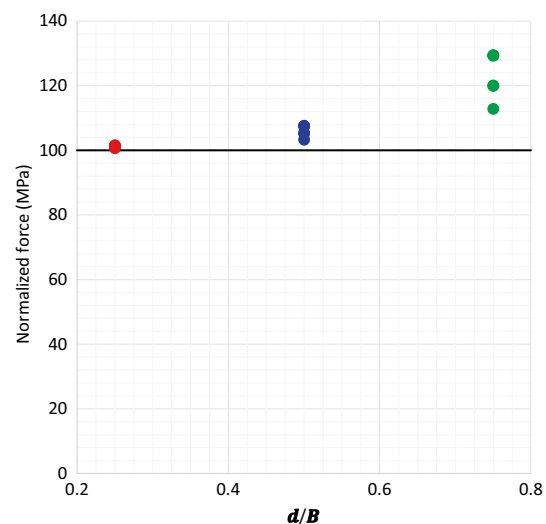


Fig. 10 Average contact pressure for all the configurations of the pin-plate coupling

We underline that this work focused on a steel coupling, but the trend of the results discussed above would be the same even for a different type of material.

A potential application of this system could be the development of a compact specimen to assess the shear strength of bonded interfaces: this can be easily obtained press fitting and bonding the pin to the plate and promoting shear stresses on the contact interface by applying a torsional load about the pin axis, by using the plate as a lever arm.

5 Conclusions

Given their widespread use in industrial applications, this work performed a numerical investigation of interference fit couplings between a perforated finite plate and a round pin, considering all the typical configurations that can be used in practice. By varying the pin diameter, the plate length, and the pin offset in the longitudinal direction, all of them normalized over plate width, we focused on a total of 18 configurations. To originate the interference between pin and plate, the finite element model applied a uniform temperature increase to the pin, calculated to generate a contact pressure equal to 100 MPa in a simplified pin-hub coupling, thus allowing a straightforward comparison and normalization of the results. The curves of the predicted contact pressure along the contact surface show a strong dependence from the pin diameter over plate width ratio, and, in addition, from the pin offset, and the plate length. A similar behaviour was observed for the equivalent von Mises stress. The comparison with photoelastic results for some specific configurations taken from the literature prove the excellent prediction by the finite element model. In addition, two stress concentration factors are provided to help designers: the first in terms of peak contact pressure, the second in terms of peak equivalent von Mises stress. These factors are calculated on the one hand over the reference contact pressure of 100 MPa, and, on the other hand, over the von Mises stress of a reference pin-hub coupling configuration with the same pin diameter over plate width ratio.

Funding Open access funding provided by Università degli Studi di Modena e Reggio Emilia within the CRUI-CARE Agreement.

Open Access This article is licensed under a Creative Commons Attribution 4.0 International License, which permits use, sharing, adaptation, distribution and reproduction in any medium or format, as long as you give appropriate credit to the original author(s) and the source, provide a link to the Creative Commons licence, and indicate if changes were made. The images or other third party material in this article are included in the article's Creative Commons licence, unless indicated otherwise in a credit line to the material. If material is not included in the article's Creative Commons licence and your intended use is not permitted by statutory regulation or exceeds the permitted use, you will

need to obtain permission directly from the copyright holder. To view a copy of this licence, visit <http://creativecommons.org/licenses/by/4.0/>.

References

1. Heywood RB (1952) Heywood.pdf. Chapman & Hall LTD, London
2. Lambert TH (1961) Elastic stresses due to an interference fit pin in a rectangular plate of finite width. *J Mechan Eng Sci* 3:236–240
3. Solodovnikov VN (1998) Effect of friction in a contact problem for a plate with a pin. *J Appl Mechan Techn Phys* 39:642–649. <https://doi.org/10.1007/BF02471263>
4. Jessop HT, Snell C, Holister GS (1957) Photoelastic investigation on plates with single interference-fit pins with load applied to plate only. *Aeronaut J* 7:297–314
5. Cox HL, Brown AFC (1964) Stresses Round Pins in Holes. *Aeronaut Quarterly* 15:357–372. <https://doi.org/10.1017/s0001925900003176>
6. Rao AK (1969) Accurate determination of interference in pin joints. *Exp Mechan* 9:45–48. <https://doi.org/10.1007/BF02327878>
7. Mather J, Baines BH (1972) Distribution of stress in axially symmetrical shrink-fit assemblies. *Wear* 21:339–360. [https://doi.org/10.1016/0043-1648\(72\)90008-7](https://doi.org/10.1016/0043-1648(72)90008-7)
8. Rao AK (1978) Elastic analysis of pin joints. *Comput Struct* 9:125–144. [https://doi.org/10.1016/0045-7949\(78\)90131-1](https://doi.org/10.1016/0045-7949(78)90131-1)
9. Murthy AV, Dattaguru B, Narayana HVL, Rao AK (1990) An improved iterative finite element solution for pin joints. *Comput Struct* 36:1121–1128. [https://doi.org/10.1016/0045-7949\(90\)90220-V](https://doi.org/10.1016/0045-7949(90)90220-V)
10. Goe RP, Guancial E (1980) Stress distributions around an interference-fit pin connection in a plated through hole. *IEEE Trans Compon Hyewds Manufact Technol Chmt* 3:392–402
11. Ciavarella M, Decuzzi P (2001) The state of stress induced by the plane frictionless cylindrical contact. I. The case of elastic similarity. *Int J Solids Struct* 38:4507–4523. [https://doi.org/10.1016/S0020-7683\(00\)00289-4](https://doi.org/10.1016/S0020-7683(00)00289-4)
12. Ciavarella M, Decuzzi P (2001) The state of stress induced by the plane frictionless cylindrical contact. II. The general case (elastic dissimilarity). *Int J Solids Struct* 38:4525–4533. [https://doi.org/10.1016/S0020-7683\(00\)00290-0](https://doi.org/10.1016/S0020-7683(00)00290-0)
13. Hou JP, Hills DA (2001) Interference contact between a pin and plate with a hole. *J Strain Anal Eng Des* 36:499–506. <https://doi.org/10.1243/0309324011514656>
14. Hou JP, Hills DA (2001) Contact between a pin and a plate with a hole under interference-fit and clearance-fit conditions. *Proc Inst Mech Eng C J Mech Eng Sci* 215:629–639. <https://doi.org/10.1243/0309324011514656>
15. Iyer K (2001) Solutions for contact in pinned connections. *Int J Solids Struct* 38:9133–9148. [https://doi.org/10.1016/S0020-7683\(01\)00054-3](https://doi.org/10.1016/S0020-7683(01)00054-3)
16. Crococolo D, Vincenzi N (2009) A generalized theory for shaft-hub couplings. *Proc Inst Mech Eng C J Mech Eng Sci* 223:2231–2239. <https://doi.org/10.1243/09544062JMES1437>
17. Pedersen P (2006) On shrink fit analysis and design. *Comput Mech* 37:121–130. <https://doi.org/10.1007/s00466-005-0664-7>
18. Strozzi A, Baldini A, Giacomini M et al (2011) Normalization of the stress concentrations at the rounded edges of a shaft-hub interference fit. *J Strain Anal Eng Des* 46:478–491. <https://doi.org/10.1177/0309324711403845>
19. Malavolta AT, Evangelista SH, Moreno ME (2013) The Influence of Thermo-Mechanical Stress State on the Torque Capacity of Rotating Interference Fit Assembly. In: 22nd International

- Congress of Mechanical Engineering (COBEM 2013). ABCM, pp 3850–3858
20. Foust BE, Lesniak JR, Rowlands RE (2014) Stress analysis of a pinned wood joint by grey-field photoelasticity. *Compos B Eng* 61:291–299. <https://doi.org/10.1016/j.compositesb.2014.01.041>
 21. Wu T, Zhang K, Cheng H et al (2016) Analytical modeling for stress distribution around interference fit holes on pinned composite plates under tensile load. *Compos B Eng* 100:176–185. <https://doi.org/10.1016/j.compositesb.2016.06.011>
 22. Imran M, Haneef M, Zameer S (2015) Interference fit simulation on pin joint by using ansys. *Int J Res Eng Technol* 04:579–583. <https://doi.org/10.15623/ijret.2015.0405107>
 23. Karmankar RG (2015) Stress analysis of interference fit by fem. *Int Res J Eng Technol (IRJET)* 2:2641–2648
 24. Pedersen NL (2019) Stress concentration and optimal design of pinned connections. *J Strain Anal Eng Des* 54:95–104. <https://doi.org/10.1177/0309324719842766>
 25. Booker JD, Truman CE (2020) Strengthening and weakening mechanisms in interference-fitted joints. In: 7th International Conference Integrity-Reliability-Failure, pp 405–418
 26. Radi E, Strozzi A (2023) Advancing contact of a 2D elastic curved beam indented by a rigid pin with clearance. *Int J Non-Linear Mech* 149:104313. <https://doi.org/10.1016/j.ijnonlinmec.2022.104313>
 27. Strozzi A, Radi E (2023) Analytical tool assisting the designer of pin-lug connections. *Proc Inst Mech Eng C J Mech Eng Sci*. <https://doi.org/10.1177/09544062231167264>
 28. Lewis R, Marshall MB, Dwyer-Joyce RS (2005) Measurement of interface pressure in interference fits. *Proc Inst Mech Eng C J Mech Eng Sci* 219:127–139. <https://doi.org/10.1243/095440605X8432>
 29. Karmankar RG (2015) Stress analysis of interference fit by FEM. *Int Res J Eng Technol* 2:2614–2648
 30. Adhithayan MA, Kumar SA, Ananth A et al (2018) Comprehensive analysis of interference fit and its attributes. *Int J Eng Res Technol (IJERT)* 6:1–5
 31. Saedi R, Sadeghi MH (2020) Investigation of insert-hole interference fit influence on downhole drilling bit failure. *Proc Inst Mech Eng B J Eng Manuf* 234:1752–1761. <https://doi.org/10.1177/0954405420927831>
 32. Gruescu CM, Davidescu A, Sticlaru C, Lovasz EC (2021) Interference fits. Bearing capacity under complex loading – FEM analysis. *Mechan Machine Sci* 88:403–414. https://doi.org/10.1007/978-3-030-60076-1_37/COVER
 33. ABAQUS User's Manual, ABAQUS/CAE 2016. <https://www.3ds.com/>. Accessed 22 Aug 2023
 34. Bower AF (2021) Applied mechanics of solids. Taylor & Francis Group, New York
 35. Budynas R, Nisbett K (2020) Shigley's mechanical engineering design. McGraw Hill, New York

Publisher's Note Springer Nature remains neutral with regard to jurisdictional claims in published maps and institutional affiliations.